JOURNAL OF MATERIALS SCIENCE 15 (1980) 1521 – 1532

Precipitation in Ni-Co-Al alloys

Part 1 *Continuous precipitation*

C. K. L. DAVIES, P. NASH*, R. N. STEVENS
Department of Materials, Queen Mary College, London E1 4NS, UK

Continuous precipitation of γ' in Ni–Co–Al alloys has been studied using X-ray diffraction, scanning electron microscopy and transmission electron microscopy. The precipitation sequence is observed to be a change of morphology from spheres → cube → plates. The $\gamma|\gamma'$ lattice parameter mismatch is of the order of 0.3%. The γ' particle growth rate has been determined over a range of temperatures for alloys containing a range of cobalt contents from 0 to 55 at %. In all cases the particle size varies at $t^{1/3}$ and the particle number density as t^{-1}. The growth rate varies very little with increasing volume fraction of γ'. The measured particle growth rate decreases with increasing cobalt content, probably as a result of partitioning of cobalt between particle and matrix. Electron microprobe analysis, volume fraction measurements and X-ray analyses were used to determine the $\gamma|(\gamma+\gamma')$ boundary in the Ni–Co–Al ternary system at temperatures between 973 and 1073 K. It is clear from the position of the boundary that a significant beneficial effect of cobalt is in decreasing the solubility of the γ' phase in γ for any temperature up to 1073 K. Histograms of particle size were constructed and compared with both the Lifshitz–Slyozov–Wagner and the Lifshitz–Slyozov encounter modified (LSEM) predicted distributions. The LSEM theory for particle coarsening was shown to be a much better fit to the experimental particle size distributions.

1. Introduction

A number of commercial nickel-based alloys hardened by γ' precipitates contain significant amounts of cobalt in the range 10 to 28 mass %. The two major contributions of this element to the properties of the alloys are said to result from the reduction of matrix stacking fault energy and the increase in the γ' solvus temperature which it causes [1]. However, no systematic study of the effects of Co addition on the growth kinetics and morphology of γ' has been reported, although this is fundamental to the service life of the alloy. Some indication of the effect may be seen by comparing the behaviour of Nimonic 80A with Nomonic 90†; the two differing in composition only in that 16 mass % Co has been substituted for Ni in the latter. At 1073 K, the γ' in Nimonic 90 grows at a considerably slower rate; with a rate constant an order of magnitude smaller than that of Nimonic 80A [1].

Since the work of Ardell and Nicholson on binary Ni–Al alloys [2, 3] the analysis of particle growth kinetics due to Lifshitz and Slyosov [4] and Wagner [5] (LSW) has been used in an attempt to describe the growth of γ' particles in a number of Ni-base alloys [6–8]. The LSW theory predicts the mean linear dimension of the particles to increase as the cube root of the time ($t^{1/3}$) and also yields on expression for the distribution of particle sizes produced by the coarsening process. While the $t^{1/3}$ law is frequently found to hold, a much wider range of particle sizes is observed experimentally. This effect is likely to be due to the effect of volume fraction of precipitate on the coarsening process as the LSW theory is only strictly applicable when the volume fraction tends to zero.

*Present address: Department of Metallurgy and Materials Science, Imperial College, London, UK.
†Trade name, Henry Wiggin Co Ltd, Hereford, UK.

0022–2461/80/061521–12$03.20/0

An attempt to modify the LSW theory by Ardell [8] to allow for the effect of volume fraction, while yielding a broader particle size distribution predicted a strong volume fraction dependence of growth rates which is not observed experimentally [2, 3, 9, 10]. Recently, a modification of the LSW theory due to Lifshitz and Slyozov, allowing for a finite volume fraction (LSEM) [4] has been developed for comparison with experimental data [11]. It was shown that the LSEM theory provided a much better fit to experimental particle size distribution and did not predict a strong effect of volume fraction of precipitate on the growth rate. The present series of alloys of varying volume fraction of γ' will therefore be used to further test the LSEM theory. At the same time, the LSEM theory will be used in an attempt to describe the role of cobalt in alloys containing a constant but not zero volume fraction of γ'.

2. Experimental procedure

Nine Ni–Co–Al alloys were prepared by vacuum melting and casting 99.99% purity starting materials. The chemically analysed compositions are shown in Table I together with the preparation methods used to produce the material in the form of 7 mm diameter rods. The alloys are designated by a code giving their nominal compositions in at %. Thus alloy Ni 37–12 contains 37 at % Co and 12 at % Al.

Specimens for hardness measurements, optical and scanning microscopy, electron microprobe analysis and X-ray diffractometry were machined from the rods, mechanically ground and polished to a 1 μm diamond finish. Solution and ageing treatments were carried out in a vertical tube vacuum furnace under a vacuum of 10^{-6} Torr followed by a water quench.

For optical microscopy, solution-treated specimens were electrolytically etched in a solution of 5% HF + 10% glycerol in water and aged specimens were etched in 2% ammonium sulphate + 2% citric acid in water. The latter etchant was also used in the preparation of carbon extraction replicas as it preferentially etches the γ matrix leaving γ' particles proud of the surface. Thin foil specimens were cut from 3 mm diameter rod and ground until approximately 0.25 mm thick with parallel faces. Thinning was carried out in a two-stage jet polishing apparatus with an electrolyte of 10% perchloric acid in ethanol.

Transmission electron microscopy was carried out on a JEOL JXA-7A microscope at 80 kV for extraction replicas. Particle size measurements were made directly on bright-field photographic plates of extraction replicas. A minimum of 400 measurements were made to obtain an average particle size and particle-size distribution. The magnification was calibrated using both latex spheres and a diffraction grating.

Electron microprobe analysis was carried out at 20 kV on a JEOL JXA-50A. The intensities of $K\alpha$ lines for all three elements were determined and compared to pure elemental standards, the results were then corrected for the effects of absorption, fluorescence and atomic number using the computer program MAGIC IV [12].

3. Results and discussion

3.1. The precipitation process

Ageing was carried out over a range of temperatures from 673 to 1123 K although only the results above 973 K are considered in detail in the present paper. In all the alloys aged at temperatures above 973 K, continuous precipitation occurred, eventually producing cube-shaped particles of γ' (Fig. 1a). At low temperatures in high cobalt alloys, precipitation occurred in a dis-

TABLE I Alloy compositions (at %)

Alloy	Ni	Co	Al	S.T. Temp (K)	Grain size (μm)	Preparation
Ni 0–13	86.7	–	13.3	1293	180	Homogenized
Ni 10–13	77.9	9.5	12.6	1293	150	24 h at 1473 K
Ni 22–13	64.9	21.7	13.4	1343	145	forged and
Ni 37–12	50.4	37.1	12.5	1293	140	swaged at 1373 K
Ni 49–12	39.3	48.7	12.0	1293	100	
Ni 9–12	78.9	9.3	11.79	1223	80	Extruded
Ni 22–11	67.1	22.1	10.77	1223	34	at 1323 K,
Ni 38–8	53.4	38.2	8.38	1223	40	homogenized 17 h
Ni 48–9	43.3	47.8	8.97	1223	67	at 1373 K, swaged at 1373 K

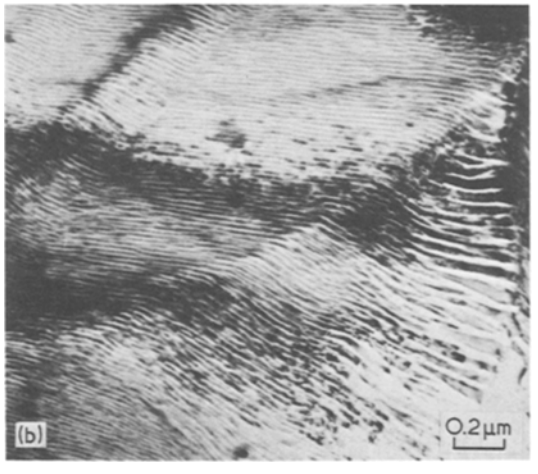

Figure 1 (a) Continuous precipitation in Ni 22–13 after ageing at 1023 K for 60 h. (b) Discontinuous precipitation in Ni 37–12 after ageing at 873 K for 0.5 h.

continuous manner producing plates of γ' (Fig. 1b). The discontinuous precipitation mode will be the subject of a later paper and only continuous precipitation will be discussed here.

The present study was not overly concerned with the early stages of precipitation. However, the limited X-ray data obtained will be presented as it has a not insignificant bearing on the coarsening process. Both matrix (γ) and precipitate (γ')

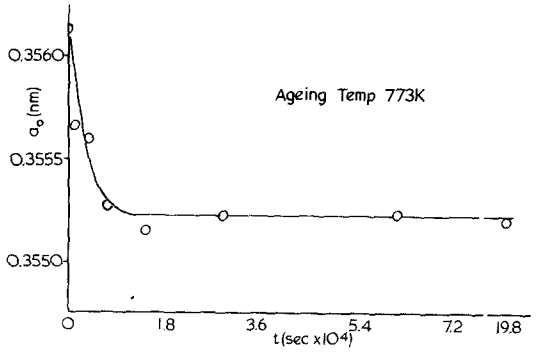

Figure 2 Matrix lattice parameter (a_0) as a function of time at 773 K for Ni 22–13.

lattice parameters were determined as a function of ageing time by powder X-ray analysis.

The matrix lattice parameter was observed to decrease rapidly from the start of ageing, quickly reaching a constant value (Fig. 2). In the period of its rapid decrease diffraction lines for the γ' precipitate appeared and grew in intensity and sharpness. The low intensity superlattice lines from the precipitate were not always observed in the early stages of ageing but appeared later. This was observed in all alloys except for Ni 37–12 at 1023 K. Side bands, previously observed for Ni–Al alloys [13], were not observed in any of the alloys including the binary Ni–Al alloys. It is probable that precipitation occurs by a classical nucleation and growth mechanism. Diffraction lines from the coherent f.c.c. γ' were used to determine γ–γ' mismatch values for several alloys (Table II), even though superlattice lines were not always observed at the earliest ageing times. It is clear that increasing cobalt content decreases the mismatch between γ' and the matrix as a result of the increasing segregation of cobalt to the matrix.

The behaviour of Ni 37–12 at 1023 K on the other hand was different suggesting a possibility that spinodal decomposition occurred in this alloy. Experiments on an X-ray diffractometer using bulk samples of Ni 37–12 aged at 1023 K, showed

TABLE II

Alloy	Temperature (K)	Phases*	% mismatch
Ni 0–13	1073	$\gamma_c - \gamma'$	0.61
Ni 22–13	873	$\gamma_c - \gamma'$	0.4
Ni 37–12	1023	$\gamma_c - \gamma'$	0.24
Ni 37–12	873	$\gamma_c - \gamma'$	0.3
Ni 49–12	873	$\gamma_c - \gamma'$	0.3

*γ_c refers to the matrix in equilibrium with continuous γ' precipitate.

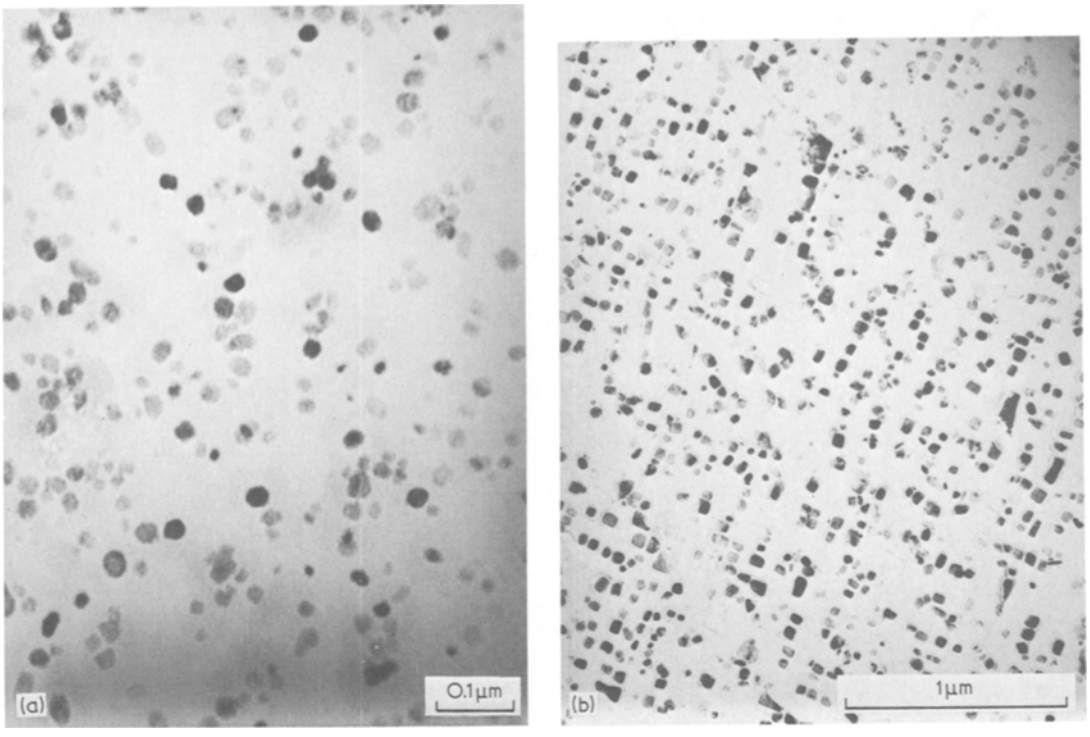

Figure 3 γ' precipitates in alloy Ni 22–11 after ageing at 973 K for (a) 40 h, (b) 320 h, showing the spherical to cubic shape change.

no shift in matrix lines at times up to 20 h nor were side bands observed. Considerable broadening of the 3 1 1 and 2 2 2 lines occurred indicating either a range of precipitate/matrix compositions or the presence of coherency stresses. On further ageing, the matrix lines shifted to lower d values and the 3 1 1 and 2 2 2 lines were observed to split into separate phases. It is possible the Ni 37–12 undergoes spinodal decomposition when aged at 1023 K. This suggestion is supported by the fact that a great deal of γ' particle interconnectivity is observed in extraction replicas obtained from aged samples of this alloy.

3.2. Morphology

The γ' morphology in these alloys after ageing at temperatures above 973 K is typical of that generally found in Ni-base superalloys and does not change significantly as a function of cobalt content. The precipitate morphology changes at an early stage from spherical to cubic (Fig. 3). The shape change is a consequence of a very low surface energy on the γ/γ' (1 0 0) planes. The particles nucleate as spheres to minimize the particle surface area per unit volume but as they grow the reduction in surface energy made by maximizing the (1 0 0) surfaces more than compensates for the increase in surface area per unit volume on changing from spheres to cubes. Gradually the precipitates become aligned forming rows of particles in ⟨1 0 0⟩ directions (Fig. 4). This is believed to be a consequence of the elastic interaction between particles as proposed by Ardell and Nicholson [2].

Coalescence of particles occurs by Ostwald ripening, as for a random spatial distribution. Coalescence can take place by long-range diffusion or by short-range diffusion following an encounter as described by Lifshitz and Slyozov [4]. Odd-shaped particles are often observed (Fig. 5) which are clearly coalesced cubes. This is good evidence for coalescence as a result of encounters. The proportion of these particles does not change significantly with time suggesting they return to their equilibrium shape by diffusion following coalescence.

Often particles can be seen to be separated by very small distances, far less than the mean particle size, without any observable effect on morphology. In other cases a bridge can be seen to have formed between particles separated by much larger distances (Fig. 6). The phenomenon of coalescence in these alloys does not, therefore,

Figure 4 Aligned rows of cubic γ' particles in Ni 22–13 after ageing for 239 h at 1073 K.

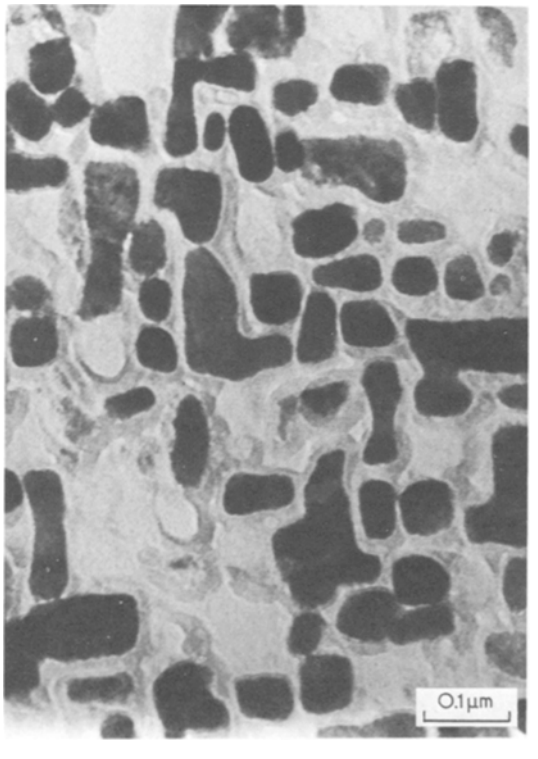

Figure 5 Odd shaped γ' particles in Ni 37–12 after ageing for 45 h at 1023 K.

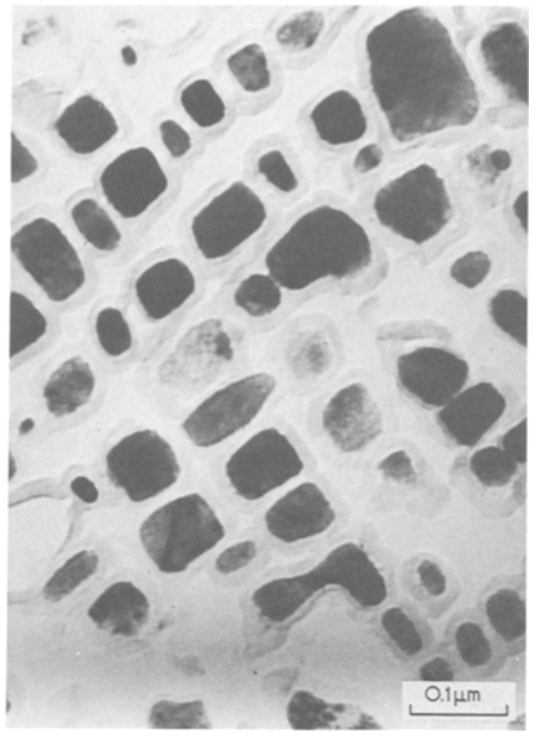

Figure 6 γ' particles in Ni 22–13 after ageing for 441 h at 973 K.

appear to be simply an effect caused by particle spacing. The particles are coherent with the matrix and have an ordered crystal structure ($L1_2$) and there is a probability of 0.5 that two adjacent particles will have their ordered structure out of phase. An antiphase boundary will have to be formed if two such particles coalesce after an encounter with an estimated antiphase-boundary energy of 220 mJ m^{-2} [14]. This would result in a net increase in energy, for coherent particles, and hence precludes coalescence of these particles at least during the early stage of ageing. However, at a later stage, the particles become incoherent and the γ/γ' surface energy may be comparable with the antiphase-boundary energy allowing coalescence of all encountering particles to occur. The possible effects of such a constraint on coalescence by encounter have not been taken into consideration in the application of the LSEM theory as applied to the results of this study.

At long ageing times, the alignment process causes the particles to coalesce to form plates as is clearly shown in the scanning electron micrograph of Fig. 7. This is contrary to the suggestion of Hagel and Beattie [15] that the equilibrium particle shape depends on mismatch. The mis-

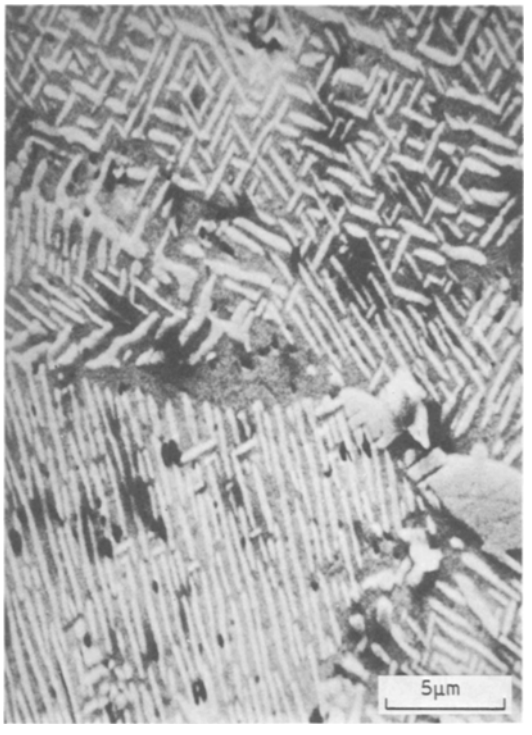

Figure 7 Plates of γ' formed in Ni 37–12 after ageing for 698 h at 1073 K.

match in these alloys is of the order of 0.3% and thus according to their proposal, particles should remain cubic. However, the mismatch may have an effect on the degree of alignment which in turn will affect the rate at which a plate-like structure is produced. This has been found to be the case for other Ni-base alloys [6].

3.3. Phase boundary

The results of the microprobe analysis and volume fraction measurements are combined in Fig. 8 where a basal projection of the Ni/Co/Al ternary equilibrium diagram is shown with $\gamma/\gamma + \gamma'$ solvus lines for various temperatures and tie lines determined for 1073 K. The phase boundaries shown correspond to a semi-coherent or incoherent solvus as the γ' compositions were determined from large γ' particles at long ageing times. The relative errors for the microprobe analysis are estimated to be ± 4% of the measured values for Ni and Co and ± 7% of the measured values for Al. Comparison between microprobe analyses and chemical analyses of solution-treated specimens indicates that the microprobe analysis gives consistently higher values for Al which is probably caused by an over-correction in the computer program.

The phase boundaries determined by Schramm [17] at 1073 K are included in Fig. 8 and show only slight deviations from the present results. The directions of the tie lines correspond well with the variation of Curie temperatures [17] with composition in this region. The Al solute contents are consistent with the X-ray lattice parameter measurements and the theoretical predictions of Moreen *et al.* [18]. It is clear from the position of the solvus boundaries determined in this study that a significant beneficial effect of Co is in decreasing the solubility of the γ' phase in γ for any given temperature up to 1073 K, and thus increasing the volume fraction of precipitate for a given aluminium content.

3.4. Particle-size distribution

Histograms of particle size are shown in Fig. 9 together with the LSW distribution and the relevant LSEM distribution. The experimental frequencies are converted to probabilities in the manner described by Ardell and Nicholson [3] except that they are not multiplied by the factor 9/4. For odd-shaped coalesced particles there is a

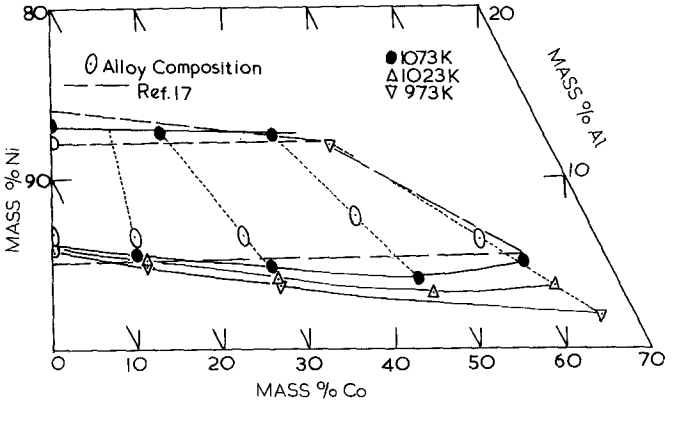

Figure 8 Partial Ni–Co–Al phase diagram showing $\gamma/\gamma + \gamma'$ solvus lines for various temperatures determined in this study.

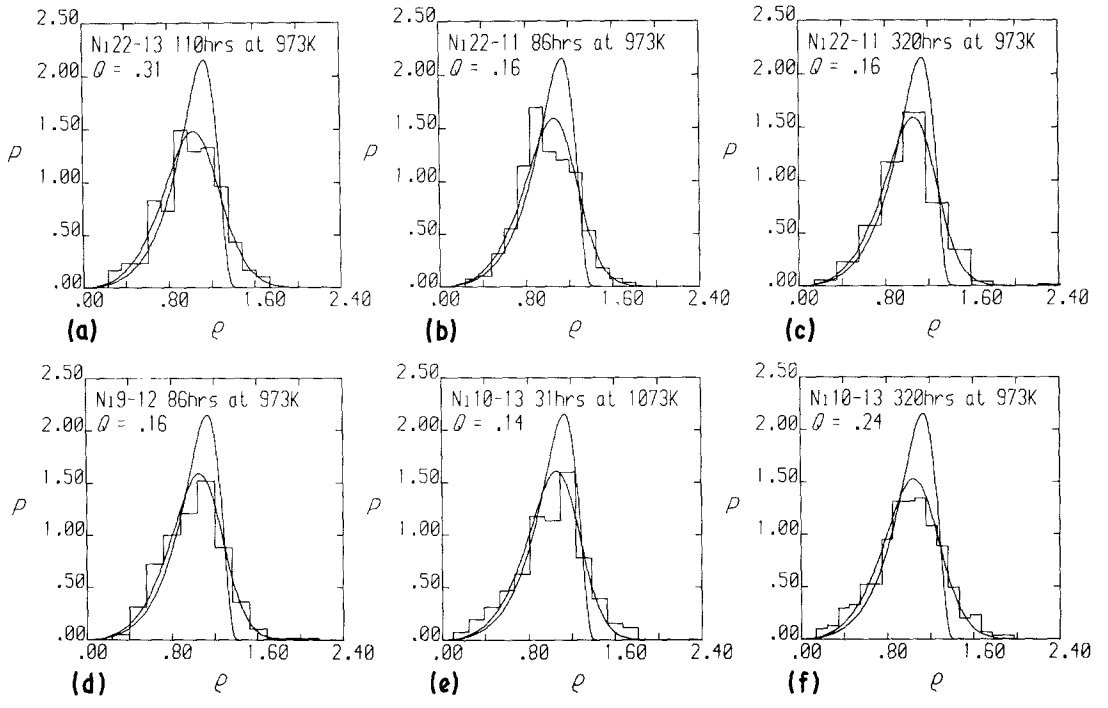

Figure 9 Comparison of the LSW and LSEM distribution function with experimental distributions for γ' type precipitates in various Ni–Co–Al alloys.

problem in defining a dimension parameter. This was approximated by dividing the particle into rectangles, assuming the depth of the particle was equal to the average of the two visible sides, summing the volumes of the separate particles, and calculating a cube edge length from the total volume. The incidence of odd-shaped particles was seen to increase with increasing γ' volume fraction but did not change with ageing time, supporting the view that these particles return to the equilibrium particle shape after encounter.

The LSW and LSEM theories predict that the particle number per unit volume, N, decreases as t^{-1} during true coarsening; when the particle size distribution is constant and the volume fraction of precipitate changes very little. Prior to this the particle number density depends on the initial precipitation process and the time taken to precipitate the equilibrium volume fraction of precipitate. Measurements of the value of N are hence a good check of the LSW and LSEM theories and can be used to determine the period taken to establish a stable particle size distribution. This incubation period tends to increase with increasing ageing temperature.

In this study N was determined from electron micrographs of extraction replicas of aged specimens by counting the number of particles per unit area. Only extracted particles present in the replica were counted as these were the only ones assumed to have their centres lying within the film. The volume in which the particles were included was calculated assuming the replica thickness was equal to the average particle size. This is a reasonable assumption only when the number of overlapping particles are small. The values of N determined are hence clearly sensitive to the experimental technique. For this reason data was cross-checked by calculating $(a^{-3}N)$ values which should show only a small increase with time. Data which did not

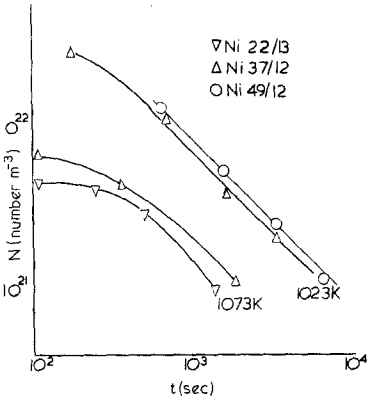

Figure 10 γ' particle number density (N) as a function of ageing time.

TABLE III

Alloy	Heat treatments t (h) at T (K)	Volume fraction γ'	Standard deviation		Coefficient of skewness		Coefficient of kurtosis	
			LSEM	Experimental	LSEM	Experimental	LSEM	Experimental
Ni 22–13	110/973K	0.31	0.283 21	0.282 31	−0.115 94	−0.295 33	0.036 319	−0.051 045
Ni 22–11	86/973K	0.16	0.261 98	0.257 0	−0.281 09	−0.037 462	0.070 923	0.036 609
Ni 22–11	320/973K	0.15	0.261 98	0.276 58	−0.281 09	0.047 973	0.070 923	0.013 039
Ni 9–12	86/973K	0.16	0.261 98	0.281 38	−0.281 09	0.148 63	0.070 923	0.467 84
Ni 10–13	30/1073K	0.14	0.259 49	0.317 31	−0.308 66	−0.280 47	0.081 198	0.032 22
Ni 10–13	320/973K	0.24	0.270 98	0.310 8	−0.186 19	−0.176 36	0.045 286	0.166 80
	LSW values		0.215 1		−0.920 0			

show this were assumed to have a large error in the value of N and were discarded.

Plots of log N versus log t are shown in Fig. 10. The values of N compare very favourably with those determined in Ni–Al binary alloys from thin foils [19]. The slopes of the straight portions of the plots have values close to -1 and hence agree with the LSW and LSEM predictions. At 1023 K a slope of -1 is evident from the earliest measured ageing times suggesting little or no incubation period with a very rapid precipitation of the full volume fraction of precipitate. At the higher temperature (1073 K) the onset of $N \propto t^{-1}$ is approached after 10^3 sec. The duration of this incubation period, during which the volume fraction of precipitate increases, is of the same order as found by Kirkwood [19].

It can be seen from the histograms in Fig. 9 that the LSEM distributions provide a far better fit to experiment than the LSW distribution. The fit improves with increasing ageing time as the particle-size distribution asymptotically approaches the theoretical distribution from the initial distribution existing after nucleation. In general the peak height, the breadth of the distribution and the general shape of the experimental histograms are well reproduced by the LSEM theory. The comparisons can be put on a more quantative basis if the standard deviations, coefficients of skewness and coefficients of kurtosis of the LSEM and LSW theoretically predicted distributions are compared to the experimental values as in Table III. The LSW values are, of course, independent of volume fraction and are given at the bottom of the table. The LSEM standard deviations are close to the experimental values and reflect the increase in breadth of the curves with increasing volume fraction of precipitate. The increase in curve width, for a constant area under the curve, necessarily decreases the peak height fitting the experimental data well. The values of the LSEM coefficients of skewness and kurtosis are much smaller than the LSW values as the curves become more symmetrical with increasing volume fraction of precipitate due to encounters. The coefficients calculated from the LSEM theory show a much better agreement with the experimental values than do to the LSW theoretical values. The improved fit for the particle-size distribution coupled with the small dependence of the rate constant on volume fraction [11] is taken as justification for using the LSEM analysis in preference to the LSW analysis to determine parameters such as σ (particle/matrix surface energy), or D (effective duffusion coefficient), from the experimentally determined rate constants.

3.5. Particle-growth kinetics

The γ' particle size ($\bar{a}$) measurements as a function of time are shown in Figs. 11 to 13. These data are

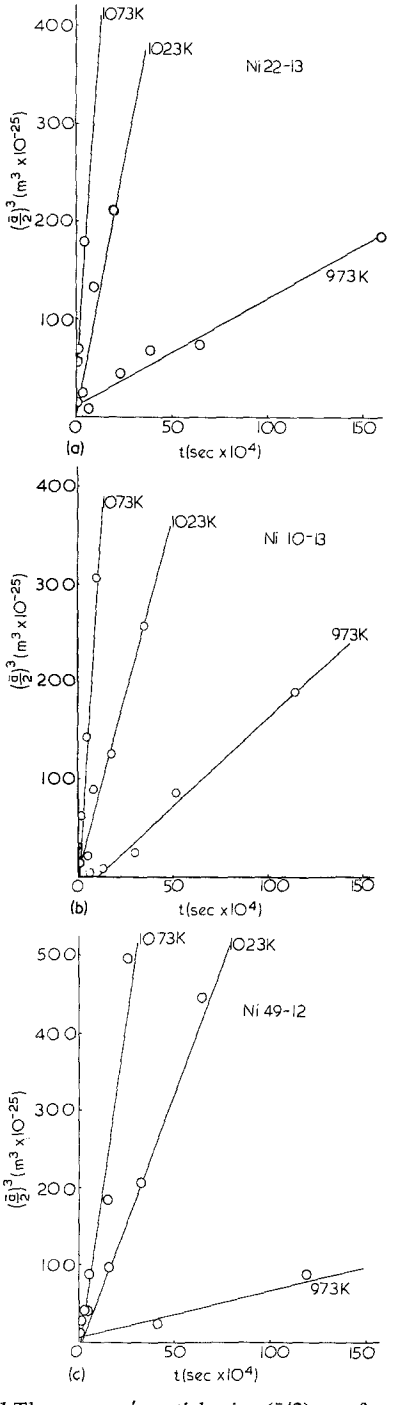

Figure 11 The mean γ' particle size ($\bar{a}/2$) as a function of ageing time and temperature for three Ni–Co–Al alloys.

plotted as $(\bar{a}/2)^3$ versus t since the factor $(\bar{a}_0/2)^3$ cannot always be neglected in the rate equation

$$\left(\frac{\bar{a}}{2}\right)^3 - \left(\frac{a_0}{2}\right)^3 = kt.$$

The straight lines were fitted by a computerized least squares method which yielded the rate constants k and the initial particle size $(a_0/2)^3$. The results are summarised in Table IV. Also shown in Table IV are values of the LSEM parameter γ which decreases with volume fraction of precipitate causing, in part, the predicted slight increase in the rate constant [11]. The $(\bar{a}_0/2)^3$ values cannot be considered meaningful, as pointed out by Ardell and Nicholson [3], since the time for nucleation and establishment of the coarsening processes is also included in the ageing time.

Before examining the effect of cobalt on the growth rate constant it is of interest to compare alloy Ni 9–12 and Ni 10–13 and alloys Ni 22–11 and Ni 22–13 at 973 K in Table IV to see if a volume fraction effect has been observed. For alloys Ni 9–12 and Ni 10–13 the higher volume fraction alloy has an experimental growth rate a factor of 1.3 greater and an LSEM predicted growth rate of a factor of 1.08 larger. For alloys Ni 22–11 and Ni 22–13 measured difference in k is a factor of 1.01 greater for the higher volume fraction alloy and a predicted factor of 1.15. This can hardly be taken as evidence of a volume fraction effect and demonstrates the problem in observing with reasonable certainty such small changes in rate constant. Comparison of alloys Ni 0–13, Ni 9–12 and Ni 22–11 at 973 K and alloys Ni 10–13, Ni 22–13 and Ni 49–12 at 973 K indicates that there is a decrease in rate constant with increasing Co content at constant volume fraction. Comparison of alloys Ni 10–13 and Ni 49–12 at 1073 K similarly indicates a decrease in growth rate constant with increasing Co. The k values in Table IV obtained at 1073 K may be compared with those of a series of Ni–Al binary alloys at the same temperature [8] which all had k values in the region of 1.1×10^{-27} m^3 sec^{-1}. Thus the addition of Co has reduced the rate constant at 1073 K by a factor of 4 to 6 depending on the Co content. Even a 10% Co addition produces a significant improvement in microstructural stability. The rate constants obtained in this study at 1073 K are comparable with those for Udimet 700 [20] and Nimonic 90 and 263 [1].

Assuming the effective diffusion coefficient D in the growth-rate equation may be given by an Arrhenius type equation then (using the LSEM analysis),

$$\log \frac{kT}{C_e} = \log \frac{6\sigma(V_m)^2(\bar{r}_c)^3 D_0}{R\gamma} - \frac{Q}{2.3RT},$$

where T is ageing temperature, C_e is the equilibrium solute content of the matrix, R is the gas constant, $\bar{r}_c^3$ and γ are parameters obtained from the LSEM analysis and depend on volume fraction of precipitate, V_m is the molar volume of precipitate, D_0 is the frequency factor and Q the activation energy for the coarsening process. Thus plots of log kT/C_e versus $1/T$ yield Q from the slope and D_0 from the intercept. Least squares fits to the data yielded the values shown in Table V. The data for alloy Ni 49–12 showed considerable scatter and the parameters derived from this plot cannot be considered accurate. The reason for the scatter in the data of

TABLE IV

Alloy	Temperature (K)	Volume fraction γ'	γ	K ($\times 10^{-30}$ m^3 sec^{-1})	$(\bar{a}_0/2)^3$ ($\times 10^{-25}$ m^3)
Ni 0–13	973	0.15	4.853	17.39	− 7.4
Ni 9–12	973	0.16	4.804	14.06	− 9.7
Ni 10–13	973	0.24	4.452	17.88	−16.4
	1023	0.17	4.755	70.85	2.12
	1073	0.14	4.903	287.0	−14.8
Ni 22–11	973	0.16	4.804	10.99	− 6.82
Ni 22–13	973	0.31	4.183	11.07	10.3
	1023	0.32	4.147	104.0	− 6.25
	1073	0.23	4.493	265.16	42.4
Ni 37–12	1023	0.45	3.712	33.12	22.9
	1073	0.35	4.041	204.4	18.75
Ni 49–12	973	0.38	3.938	6.18	6.4
	1023	0.27	4.333	67.2	− 9.3
	1073	0.15	4.853	179.75	−28.7

TABLE V

Alloy	Q ($\times 10^3$ J mol^{-1})	C_e($\times 10^4$ mol)	D_0(m^2 sec^{-1})	D ($\times 10^{-17}$ m^2 sec^{-1})
Ni 10–13	239	1.66	8.4×10^{-6}	1.92
Ni 22–13	264.5	1.48	2.0×10^{-4}	2.63
Ni 49–12	219.4	1.54	8.4×10^{-7}	1.74

alloy Ni 49–12 may lie in the fact that the 973 K datum point lies below the Curie temperature of this alloy [17]. It has been shown that there is a diffusion anomaly over a temperature range around the Curie temperature [21] and therefore the k values used in the log kT/C_e versus $1/T$ plots may not lie on the same straight line. The diffusivities determined in Table V are for a temperature of 1073 K and assume a value for σ of 8 mJ m^{-2}; they compare well with the value of 2.1×10^{-17} m^2 sec^{-1} obtained for binary Ni–Al by extrapolating the data of Swalin and Martin [22] down to 1073 K. It is difficult to ascribe unambiguously a single reason to the role of cobalt in decreasing the particle growth rate at constant volume fraction. The major effect is probably the change in the effect diffusion coefficient due to the partitioning of cobalt between particle and matrix.

In the absence of diffusion data for the ternary alloys the γ/γ' interfacial energy may only be estimated in the binary Ni–Al alloy. The molar volume was taken to be that of the stoichiometric Ni_3Al $L1_2$ structure and the diffusion coefficient at 973 K was obtained by extrapolation of published data. Using the experimental growth rate and the relevant value of $\bar{r}_c^3/\gamma$ the value of σ was calculated to be 8.9 mJ m^{-2} whilst from the LSW growth equation a value of 12.4 mJ m^{-2} was obtained. These values compare well with that obtained by Ardell [23] of 14.3 mJ m^{-2} using solute concentration and particle size measurements. In view of the preceding discussion the value of 8.9 mJ m^{-2} is believed to be a better estimate of the γ/γ' surface energy.

4. Conclusions

Precipitation in these alloys occurs by a classical nucleation and growth mechanism with a precipitate sequence of spheres → cubes → plates. The particle/matrix lattice parameter mismatch is of the order of 0.3%.

The particle size in all the alloys varies as $t^{1/3}$ and the particle number density as t^{-1}. The Lifshitz–Slyozov encounter modified particle coarsening theory (LSEM) has been shown to be a better fit to the experimental particle size distributions than the LSW theory.

The experimental rate constants show only a small dependence of particle volume fraction as predicted by the LSEM theory [11]. Particle-growth rates were found to decrease with cobalt content at a constant particle volume fraction. This is probably largely due to the time taken to partition cobalt between matrix and particle. It is clear from the position of the solvus boundaries for the Ni–Co–Al ternary diagram, determined in this study, that cobalt has a significant effect in decreasing the solubility of the γ' phase in γ for any temperature up to 1073 K.

Acknowledgements

The authors would like to thank the Science Research Council for the grant that enabled this work to be carried out. One of the authors, P. Nash owes thanks to the SRC for the maintenance grant which covered the period of this work. Thanks are also due to Delta Metals, Ipswich, International Nickel, Birmingham and the National Physical Laboratory for assistance in melting and forming the alloys.

References

1. W. BETTERIDGE and J. HESLOP, "The Nimonic Alloys", (Edward Arnold, London, 1974) p. 45.
2. A. J. ARDELL and R. B. NICHOLSON, *Acta Met.* **14** (1966) 1295.
3. *Idem, J. Phys. Chem. Solids* **27** (1966) 1793.
4. I. M. LIFSHITZ and V. V. SLYOZOV, *ibid.* **19** (1961) 1935.
5. C. WAGNER, *Z. Electrochem.* **65** (1961) 581.
6. V. BIS and D. L. SPONSELLER, *Met. Trans.* **4** (1973) 1953.
7. E. H. VAN DER MOLEN, J. M. OBLACK and O. H. KRIEGE, *ibid.* **2** (1971) 1627.
8. A. J. ARDELL, *ibid.* **20** (1972) 611.
9. S. SARIAN and H. W. WEART, *J. Appl. Phys.* **34** (1966) 323.
10. G. R. SPEICH and R. A. ORIANI, *Trans. Met. Soc. AIME* **233** (1965) 623.
11. C. K. L. DAVIES, P. G. NASH and R. N. STEVENS, *Acta Met.* **28** (1980) 179.
12. J. W. COLBY, "Advances in X-ray Analysis", Vol. 11 (Plenum Press, New York, 1968) p. 287.

13. I. A. BAGARIATSKII and I. D. TIAPKIN, *Sov. Phys. Cryst.* **2** (1957) 414.
14. P. A. FLINN, *Trans. AIME* **218** (1960) 145.
15. W. C. HAGEL and H. J. BEATTIE, *ibid.* **215** (1959) 967.
16. D. E. LAUGHLIN, *Acta Met.* **24** (1976) 53.
17. J. SCHRAMM, *Z. Metallk.* **33** (1941) 403.
18. H. A. MOREEN, R. TAGGART and D. H. POLONIS, *Met. Trans.* **2** (1971) 265.
19. D. H. KIRKWOOD, *Acta Met.* **18** (1970) 563.
20. R. STICKLER, "High Temperature Materials in Gas Turbines", (Elsevier, Oxford, 1974) p. 115.
21. K. HIRANO, R. P AGARWALA, B. L. AVERBACH and M. COHEN, *J. Appl. Phys.* **33** (1962) 3049.
22. R. A. SWALIN and A. MARTIN, *Trans. AIME* **206** (1956) 567.
23. A. J. ARDELL, *Acta Met.* **16** (1968) 511.

Received 19 October and accepted 9 November 1979.